

# A Miniaturized Low Pass Filter with Extended Stopband and High Passband Selectivity

Pankaj Singh TOMAR, Manoj Singh PARIHAR

Dept. of Electronics and Communication Engineering, Indian Institute of Information Technology Design and Manufacturing (IIITDM) Jabalpur, India

1822606@iiitdmj.ac.in, mparihar@iiitdmj.ac.in

Submitted January 9, 2023 / Accepted May 24, 2023 / Online first July 31, 2023

**Abstract.** *In this work, an ultra-wide stopband low pass filter (LPF) with high selectivity is proposed using coupled stepped impedance resonators (SIRs), open shunt stubs and circular slots in the ground plane. The proposed LPF has been modeled using a lumped equivalent circuit which is extracted from the EM model. The design has been validated through the simulation and experimental results. The fabricated prototype has a 3-dB cutoff frequency ( $f_c$ ) of 2.44 GHz and an ultra-wide stopband extended up to 20.5 GHz ( $8.4 f_c$ ) with an attenuation level  $> 20$  dB. The transition bandwidth (from 3 dB to 20 dB) is 0.09 GHz and the roll-off rate is 225 dB/GHz (reference to 30 dB). The passband insertion loss is 0.35 dB at 1.22 GHz and the normalized circuit size of the filter is 0.045.*

## Keywords

Ground slot with via, open shunt stubs, roll-off rate, step impedance resonator, ultra-wide stopband

## 1. Introduction

A compact and low-profile low-pass filter (LPF) is crucial for realizing an efficient wireless communication system by eliminating spurious and undesired higher-order frequency components. In order to achieve seamless and reliable communication, the LPF must possess several key features, including high passband selectivity, a wide stopband rejection capability, low passband insertion loss, and strong attenuation in the stopband. There have been numerous design methodologies and techniques proposed so far to achieve the desired characteristics of LPF. The use of planar resonator circuits, particularly based on microstrip technology is widely popular in designing low-pass filters due to their compact size, ease of fabrication, and ability to integrate with other high-frequency devices and circuits. The recent articles have reported various circuit topologies of the LPFs, which have been analyzed in detail based on several parameters such as roll-off rate (ROR), stopband bandwidth (SB), out-of-band rejection, and passband insertion loss (IL) [1–13]. In [1], a number of microstrip filters are reported to miniaturize the size. The LPF proposed in

[2] has employed a coupled line hairpin unit to achieve a low pass response with a wide stopband, although the roll-off rate did not meet the required specifications. A radial resonator is used in the LPF circuit described in [3] to achieve a sharper roll-off rate, albeit with a limited stopband bandwidth. In [4], T-shaped resonator is utilized for achieving a wide stopband and low insertion loss simultaneously. In [5] multiple transmission zeros are created using SIR stubs in the stopband. A filter based on microstrip stepped-impedance polygonal patch resonators is reported in [6] to achieve sharp transition band but with narrow stopband. In [7], symmetrically patches loaded LPF is proposed to for ultra-wide stopband. In [8], a defected ground c-shaped structure is employed to achieve a wide stop bandwidth, but exhibits high radiation losses in the stopband. The wide stopband can be achieved in LPF by using a lattice-shaped resonator, as proposed in [9]. A very high selectivity/roll-off rate LPF is realized in [10], although the stopband is insubstantial and in-band impedance matching is poor. In [11], a radial open stub and a butterfly open stub resonators are used to improve the stop bandwidth of conventional LPF, but it has a complex design. A LPF with improved roll-off rate is achieved using SIRs and multiple rectangular stubs at low cutoff frequency in [12]. (It is relatively more challenging to obtain a high roll-off rate when the operating frequency is higher). In [13], a LPF with an exceptionally wide stopband is proposed through a pair of SIR, open stubs and ground slots although it shows a poor roll-off rate which needs to be improved further for better passband selectivity. Besides none of the reported LPFs can achieve size compactness, high roll-off rate, and wide stopband features simultaneously and altogether. In this article a highly miniaturized LPF for RF frontend application is proposed which offers improved the roll-off rate ( $\zeta$ ) using the technique of coupled SIRs and has very compact size realized due to meandering of the inductive lines. The stopband band bandwidth has been enhanced through a pair of quarter-wave open stubs and two circular ground slots which act as stopband series resonators and as stopband circular cavity parallel resonators, respectively.

The manuscript is structured in the following manner: Section 2 describes the design of a microstrip low pass filter, followed by an analysis of simulated results. Section 3

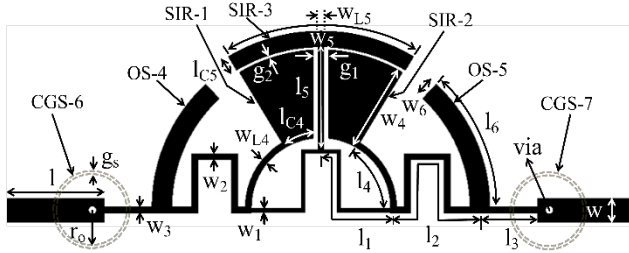


Fig. 1. The proposed design layout of a low pass filter.

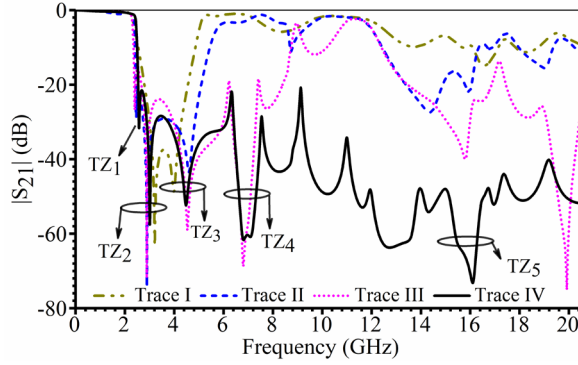


Fig. 2. Transmission coefficient: Trace I - with SIR-1&2, Trace II - adding SIR-3, Trace III - adding OS-4&5, Trace IV - with CGS-6&7.

demonstrates the extraction of the lumped circuit model using numerically calculated lumped parameters followed by the validation with the EM model. In Sec. 4, the measured results are discussed and compared with other published work with detailed performance analysis. Finally, the key findings of the work are presented in Sec. 5.

## 2. Proposed Low Pass Filter Design

The proposed low-pass filter (LPF) is depicted in Fig. 1, which illustrates the design layout of the filter. The preliminary design of the circuit comprises two stepped impedance resonators (SIR-1 & SIR-2) that are electrically coupled and connected to a high impedance (inductive) line connecting the input and output feeds. To miniaturize the size the inductive line has been meandered which results in 35% reduction in normalized circuit size. The tapered low-impedance (capacitive) lines are designed with a gap ( $g_1$ ), which offers capacitive coupling between SIR-1 and SIR-2, resulting in a low-pass filtering response with two transmission zeros (TZ<sub>2</sub> & TZ<sub>3</sub>). The response and performance of the initial circuit (Fig. 2, Trace I) is quantified by a roll-off rate/selectivity of 40.4 dB/GHz and stopband of 4.55 GHz. With an operating frequency of 2.44 GHz, the circuit generates two transmission zeros, TZ<sub>2</sub> and TZ<sub>3</sub>, at frequencies of 3.0 GHz and 4.47 GHz, respectively. To improve the selectivity an additional T-shaped resonator (SIR-3) has been inserted between SIR-1 & SIR-2 and tightly coupled to them through gap  $g_2$ . Due to the enhanced coupling and generation of additional transmission zeros (TZ<sub>1</sub> @ 2.57 GHz) close to the cutoff frequency, the roll-off rate is considerably improved as shown in

Trace II, but the stopband is still limited (up to 5.1 GHz). The improvement in the stopband bandwidth of the circuit is achieved by introducing a pair of quarter-wave open stubs (OS-4&5) in the shunt to the high impedance lines (inductive lines). The open stubs create a new transmission zero, TZ<sub>4</sub>, at 6.8 GHz that extends the stopband up to 8.4 GHz with an attenuation level better than 16 dB, as demonstrated in Trace III. With the goal of enhancing the rejection bandwidth further and to increase the stopband attenuation level, a pair of two circular ground slots (CGS-6 and CGS-7) of the same size is etched in the ground plane. These slots are connected to the centers of the input and output feed lines through the vias, which further improve the stopband of the circuit. The circular ground slots, CGS-6 and CGS-7, act as resonators that create a transmission zero (TZ<sub>5</sub>) at 16 GHz, which significantly widens the stopband and enhances the circuit's ability to block out-of-band signals, as demonstrated in Trace IV of Fig. 2. As evident the circuit's roll-off rate is significantly improved to 225 dB/GHz, and the stopband has been extended up to 20.5 GHz with an attenuation level of at least 20 dB throughout the entire stopband.

## 3. Investigation and Circuit Modeling

To understand the design principle and to obtain a better physical insight, first an LC circuit/lumped equivalent has been extracted as shown in Fig. 3. The lumped/LC elements are related to their distributed CST EM model as shown in Fig. 1 through (1), (2), derived using quasi-lumped analysis technique [1]. Here,  $f_c$  is LPF cutoff frequency and  $\beta_h$ ,  $\beta_l$  are the phase constant corresponding to thin (high impedance  $Z_h$ ) and thick (low impedance  $Z_l$ ) lines, respectively. Equation (3) is used to calculate the values of  $L_6$  and  $C_6$  corresponding to the transmission zero ( $f_{TZ4}$ ) and characteristic impedance ( $Z_6$ ), for the length and width of open stubs. Equation (4) is used to calculate transmission zero ( $f_{TZ4}$ ) which is created by quarter wavelength open stubs. Equation (5) is used to calculate transmission zero ( $f_{TZ5}$ ) for the radius ( $r_0$ ) of circular slots.

$$L_{1,2,3,4,5} = \frac{l_{1,2,3,4,5} \beta_{h_{1,2,3,4,5}} Z_{h_{1,2,3,4,5}}}{2\pi f_c}, \quad (1)$$

$$C_{4,5} = \frac{l_{c_{4,5}} \beta_{l_{4,5}}}{2\pi f_c Z_{l_{4,5}}}, \quad (2)$$

$$C_6 = \frac{1}{2\pi f_{TZ4} Z_6}, \quad L_6 = \frac{Z_6}{2\pi f_{TZ4}}, \quad (3)$$

$$f_{TZ4} = \frac{c}{4l_6 \sqrt{\epsilon_{r,eff}}}, \quad (4)$$

$$f_{TZ5} = \frac{1.8114 c}{2\pi r_0 \sqrt{\epsilon_r}} \quad (5)$$

where  $c$  is speed of light.

Model	Parameters
Distributed EM model	$l_1=6.61, w_1=0.2, Z_{h1}=116.57, l_2=9.25, w_2=0.3, Z_{h2}=100.38, l_3=2.9, w_3=0.3, Z_{h3}=100.38, l_4=3.6, w_{14}=0.3, Z_{h4}=100.38, l_{c4}=1.495, w_4=4.45, Z_{i4}=43.06, l_5=5.19, w_{15}=0.3, Z_{h5}=100.38, l_{c5}=0.8, w_5=9.8, Z_{i5}=9.42, l_6=6.97, w_6=1, Z_6=55.65, g_1=0.8, g_2=0.3, g_3=0.2, r_{via}=0.2, r_6=2.7, l=9.4, w=1.19$ [ $l_i, w_i, g_s, r_i$ in mm and $Z_{h_i}, Z_{i_i}$ in $\Omega$ ]
Calculated Lumped (LC) model	$L_1=3.993, L_2=4.849, L_3=1.52, L_4=1.887, C_4=0.568, L_5=2.72, C_5=0.54, C_g=0.11, L_6=1.337, C_6=0.4318, L_7=0.074, C_7=0.409, L_8=0.2353, C_8=1.5496$ [ $L$ in nH and $C$ in pF]
Optimized Lumped (LC) model	$L_1=3.6, L_2=2.5, L_3=0.4, L_4=2.3, C_4=1.0, L_5=1.1, C_5=1.7, C_g=0.075, L_6=1.28, C_6=0.42, L_7=0.034, C_7=1.06, L_8=0.074, C_8=0.409$ [ $L$ in nH and $C$ in pF]

Tab. 1. EM and distributed model parameters.

The physical dimensions of distributed/EM model, numerically calculated and optimized values of lumped equivalent are provided in Tab. 1. It could be observed that the optimized L, and C values are in fair agreement with numerically calculated values. The transmission zeros (TZ<sub>4,5</sub>) due to open stubs and circular ground slots can be clearly expressed through (4), (5), respectively. However, to predict the location (frequency) of TZ<sub>1</sub>, TZ<sub>2</sub>, TZ<sub>3</sub>, and TZ<sub>4</sub>, an even-odd mode analysis has been applied to the basic LC equivalent circuit along the imaginary line PQ (axis of symmetry) shown in Fig. 3. Along the axis PQ (axis of symmetry) the LC circuit has been employed as open- and short-circuits when examining even- and odd-modes, respectively. Figures 4(a) and (b) show the open- and short-circuited lumped model for even and odd modes respectively along the PQ axis. The even and odd mode impedances are expressed by (6), (7) respectively, which are derived from Fig. 4(a), (b) respectively to determine the location of the TZ<sub>1,2,3,4</sub> accurately.

Even mode impedance:

$$Z_{(in)e} = j\omega L_3 + \frac{Z_A Z_B}{(Z_A + Z_B)} \tag{6}$$

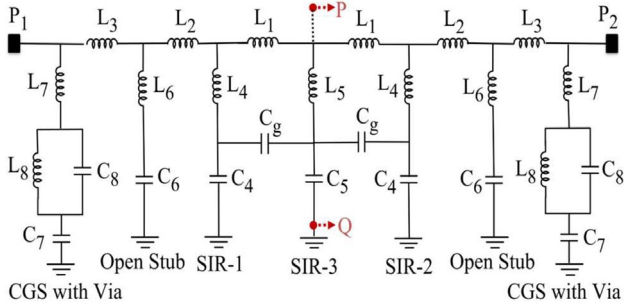


Fig. 3. Equivalent lumped circuit model of the proposed LPF.

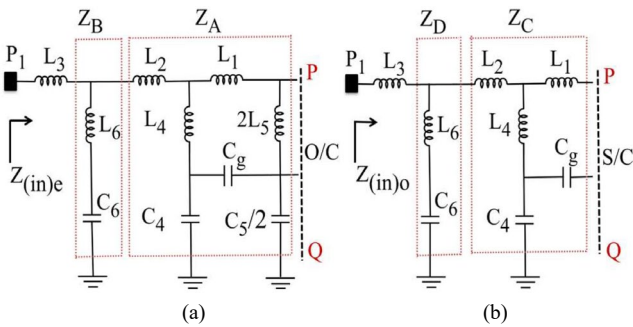


Fig. 4. (a) Even mode, (b) odd mode of the distributed model.

where

$$Z_A = j\omega L_2 + \frac{1}{j\omega C_Z} + \frac{(1 - \omega^2 L_4 C_X) [1 - \omega^2 (L_1 + 2L_5) C_Y]}{j\omega [(C_X + C_Y) - C_X C_Y (L_1 + L_4 + 2L_5) \omega^2]}$$

$$C_X = C_4 + C_g + \frac{2C_4 C_g}{C_5}, \quad C_Y = C_g + \frac{C_5}{2} + \frac{C_g C_5}{2C_4},$$

$$C_Z = C_4 + \frac{C_5}{2} + \frac{C_4 C_5}{2C_g},$$

$$Z_B = j\omega L_6 + \frac{1}{j\omega C_6}$$

where Z<sub>A</sub> and Z<sub>B</sub> are intermediary impedances in even mode circuit, which are indicated by the dotted lines of Fig. 4(a).

Odd mode impedance:

$$Z_{(in)o} = j\omega L_3 + \frac{Z_C Z_D}{(Z_C + Z_D)} \tag{7}$$

where

$$Z_C = \frac{j\omega [(L_1 + L_2) - \omega^2 (L_1 L_2 + L_2 L_4 + L_4 L_1) (C_4 + C_g)]}{[1 - \omega^2 (L_1 + L_2) (C_4 + C_g)]},$$

$$Z_D = j\omega L_6 + \frac{1}{j\omega C_6}$$

where Z<sub>C</sub> and Z<sub>D</sub> are intermediary impedances in odd mode circuits, which are indicated by the dotted lines of Fig. 4(b).

$$S_{21} = \frac{(Z_{(in)e} - Z_{(in)o}) Z_o}{((Z_{(in)e} + Z_{(in)o}) / 2 + Z_o)^2 - ((Z_{(in)e} - Z_{(in)o}) / 2)^2}, \tag{8}$$

$$S_{21} |_{\omega=2\pi f_{TZ1,2,3,4}} = 0,$$

$$(Z_{(in)e} - Z_{(in)o}) |_{\omega=2\pi f_{TZ1,2,3,4}} = 0,$$

$$(Z_A - Z_C) |_{\omega=2\pi f_{TZ1,2,3}} = 0, \tag{9}$$

$$Z_B |_{\omega=2\pi f_{TZ4}} = 0. \tag{10}$$

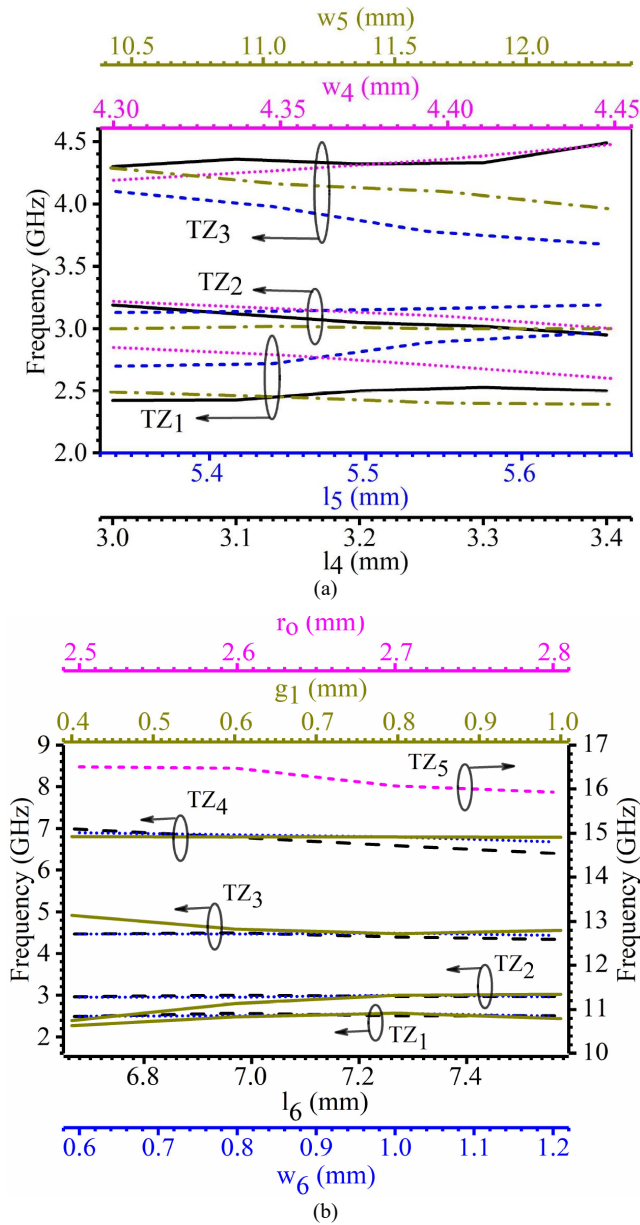


Fig. 5. Variation of transmission zero with distributed parameters (a)  $l_4$ ,  $l_5$ ,  $w_4$ ,  $w_5$ , (b)  $l_6$ ,  $w_6$ ,  $g_1$ ,  $r_0$ .

The position of transmission zeros could be estimated by putting  $S_{21}$  equal to zero in (8). The calculated values of frequencies of transmission zeros (TZ<sub>1,2,3</sub>) are 2.57 GHz, 2.98 GHz, and 4.48 GHz, which are obtained from (9), and the frequency of TZ<sub>4</sub>, which is 6.68 GHz, is calculated from (10) by putting the values of  $Z_A$ ,  $Z_B$ ,  $Z_C$ , and  $Z_D$ . These calculated values of transmission zeros are nearly close to the corresponding values of the EM model. The circular ground slots are not included in the even-odd mode analysis of the proposed model shown in Fig. 4, because they generate transmission zero independently at 16 GHz (TZ<sub>5</sub>). The metallic patch of circular slots in the ground plane acts as cylindrical cavity and is modelled as parallel bandstop resonator. To find the resonance, the boundary condition is applied at the edge of the circular conductor inside the circular slot of cylindrical cavity resonator. Therefore, the radial component of the surface current at the edge of the

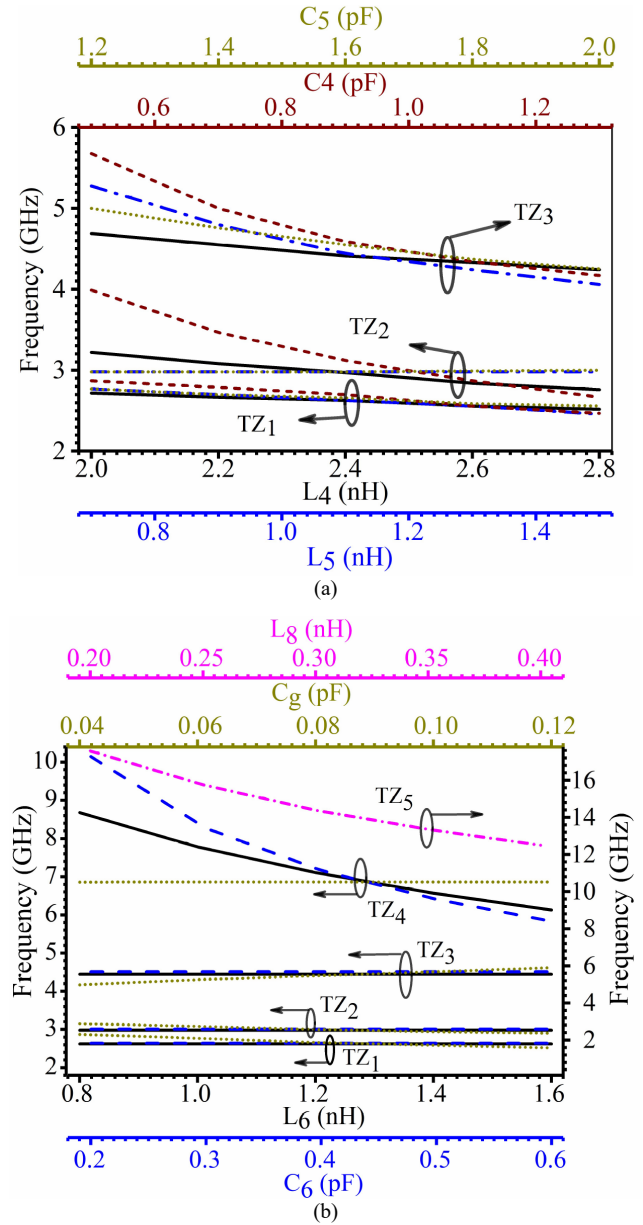


Fig. 6. Variation of transmission zero with lumped parameters (a)  $L_4$ ,  $L_5$ ,  $C_4$ ,  $C_5$ , (b)  $L_6$ ,  $C_6$ ,  $C_g$ ,  $L_8$ .

plane inside the circular slot must vanish [1]. This concept develops the stopband characteristics of circular ground slots and the resonance frequency of TZ<sub>5</sub> (for the dominant mode) is expressed by (5). Circular slot with via functions as a band stop circuit that creates transmission zero with large stopband (The detailed principal and related expressions are provided in Appendix A).

To observe the sensitivity of the filter's response with the physical dimensions, a parametric study is carried out as shown in Fig. 5(a), (b). It is noticed from here that TZ<sub>1</sub> is constant with  $l_4$  and  $w_4$  and varies considerably with  $l_5$  and  $w_5$ . TZ<sub>2</sub> primarily depends on  $w_4$  and  $l_4$ . It is also observed that TZ<sub>3</sub> varies considerably with  $l_5$  and  $w_5$ . TZ<sub>3</sub> varies sharply with change in  $g_1$ . TZ<sub>2</sub> and TZ<sub>3</sub> are reached near to each other for the large gap  $g_1$  (or smaller values of  $l_{c4}$ ) and move apart as the gap  $g_1$  reduces (length of  $l_{c4}$  increases).

TZ<sub>4</sub> primarily varies on length of open stubs  $l_6$  and TZ<sub>5</sub> varies with the radius of the ground slot  $r_o$ . The lumped parameters of the LC equivalent circuits also exhibit a similar kind of variation as shown in Fig. 6(a), (b) which justify the equivalent circuit of the EM model.

### 4. Result and Discussion

The proposed LPF design is implemented on a Rogers 3380 substrate, which has a dielectric constant of 3.38, loss

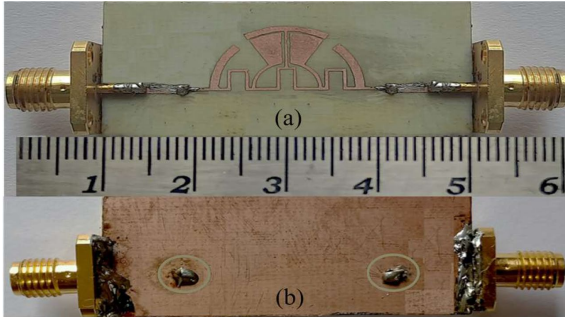


Fig. 7. Photograph of fabricated LPF: (a) Top layer, (b) bottom layer.

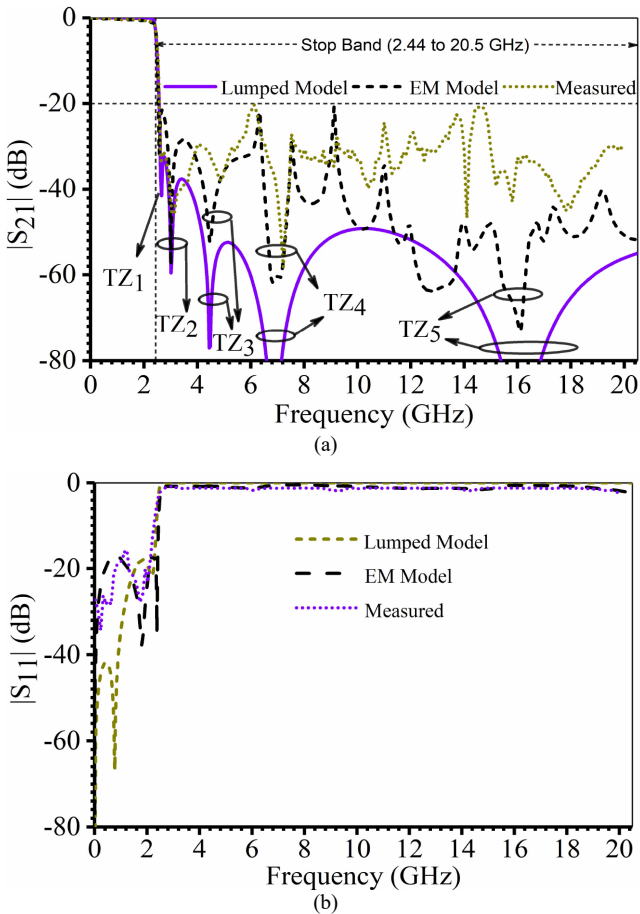


Fig. 8. Simulated and measured results of (a) S<sub>21</sub> parameter, (b) S<sub>11</sub> parameter.

Ref.	$f_c$ [GHz]	RL [dB]	IL [dB]	$\xi$ @30 dB [dB/GHz]	SF	SB > 20 dB	NCS
[4]	2.68	18.5	0.12	51	2.0	8.2 $f_c$	0.223
[5]	0.90	15.5	0.5	57	2.2	17.6 $f_c$	0.018
[6]	2.28	18.0	NA	108	2.0	3.73 $f_c$	0.054
[7]	2.44	17.7	NA	93	2.0	5.39 $f_c$	0.038
[8]	1.56	15.7	0.32	123	2.0	11.7 $f_c$	0.067
[10]	2.45	18	0.85	108	2.0	7.09 $f_c$	0.033
[11]	1.12	14.4	0.3	201	2.2	12 $f_c$	0.012
[13]	2.92	18	0.32	112	2.0	8.8 $f_c$	0.056
<b>PW</b>	<b>2.44</b>	<b>16</b>	<b>0.35</b>	<b>225</b>	<b>2.0</b>	<b>8.4<math>f_c</math></b>	<b>0.045</b>

Tab. 2. Comparison of the proposed work (PW) with previous LPF<sub>s</sub> work.

tangent of 0.0027, substrate height of 0.51 mm, and metal cladding thickness of 17.5 microns. A conventional lithography process has been used for the fabrication. Figure 7 depicts the top and bottom layers of the fabricated prototype LPF. To measure the performance of the filter, a Keysight Vector Network Analyzer (E5071 model) is used which provides the transmission and reflection coefficients.

The results obtained from the CST EM simulator are compared to the measured results, as shown in Fig. 8(a), (b). It could be observed that the measured results are showing a good agreement with the EM model in the desired band of operation. However, a slight deviation is observed between the simulated and measured results and that might be due to the fabrication tolerance and measurement uncertainties. The LPF prototype that has been fabricated demonstrates a cutoff frequency ( $f_c$ ) of 2.44 GHz, a roll-off rate ( $\xi$ ) of 225 dB/GHz, and an ultra-wide stopband (SB) that extends from the 3 dB cutoff point at 2.44 GHz to 20.5 GHz, which is 8.4 times of the cut-off/operating frequency. The LPF has a passband-to-stopband transition bandwidth of 0.09 GHz. In addition, the passband insertion loss (IL) and return loss (RL) are both less than 0.35 dB and better than 16 dB, respectively. The suppression level in the whole stopband is better than 20 dB. Suppression factor (SF) is better than 2. The LPF has a physical circuit size of 21.8 × 9.64 mm<sup>2</sup> and a normalized circuit size (NCS) of 0.045 with reference to the guide wavelength. A comparison of the proposed LPF with other relevant works is presented in Tab. 2. The proposed LPF exhibits better performance in terms of roll-off rate/selectivity, stopband bandwidth, and compactness. Besides it provides a better trade-off between all these performance parameters.

Roll-off rate ( $\xi$ ) is defined as:

$$\xi = \frac{\alpha_{max} - \alpha_{min}}{f_s - f_c} \text{ dB / GHz} \tag{11}$$

where  $\alpha_{max}$  = 30 dB,  $\alpha_{min}$  = 3 dB and the initial frequency,  $f_s$ , has a 30 dB attenuation.

## 5. Conclusion

In this paper, a new and compact design of low pass filter (LPF) has been presented that incorporates three coupled stepped-impedance resonators (SIRs), a pair of open stubs, and a pair of circular slots in the ground plane. The deployment of SIRs and their strong electrical coupling has led to a significant improvement in the roll-off rate of the filter. Furthermore, the integration of a pair of open stubs and a pair of circular slots in the ground plane contributes to achieving an ultra-wide stopband with improved attenuation/rejection level. The equivalent lumped LC circuit model has been applied to thoroughly investigate the proposed circuit and accurately estimate the locations of transmission zeros. The fabricated prototype exhibits a high roll-off rate of 225 dB/GHz, an ultra-wide stopband extending up to 20.5 GHz (8.4 $f_c$ ), and a compact normalized circuit size of 0.045. The LPF prototype demonstrates passband insertion loss of less than 0.35 dB and stopband attenuation levels of more than 20 dB. It is believed that the LPF presented in this work is expected to have an excellent spurious signal rejection capability, making it well-suited for the front-end RF applications.

## References

- [1] HONG, J. S. *Microstrip Filters for RF/Microwave Application*. 2<sup>nd</sup> ed., New York (USA): John Wiley & Sons, Inc., 2011. ISBN: 9780470408773
- [2] WEI, F., CHEN, L., SHI, X. W. Compact lowpass filter based on coupled-line hairpin unit. *Electronic Letters*, 2012, vol. 48, no. 7, p. 379–381. DOI: 10.1049/el.2011.3811
- [3] HAYATI, M., NADERI, S., JAFARI, F. Compact microstrip lowpass filter with sharp roll-off using radial resonator. *Electronic Letters*, 2014, vol. 50, no. 10, p. 761–762. DOI: 10.1049/el.2014.0648
- [4] SHEIKHI, A., ALIPOUR, A., ABDIPOUR, A. Design of compact wide stopband microstrip low-pass filter using T-shaped resonator. *IEEE Microwave Wireless Component Letters*, 2017, vol. 27, no. 2, p. 111–113. DOI: 10.1109/LMWC.2017.2652862
- [5] CHEN, F., LI, R., CHU, Q. Ultra-wide stopband low-pass filter using multiple transmission zeros. *IEEE Access*, 2017, vol. 5, p. 6437–6443. DOI: 10.1109/ACCESS.2017.2693344
- [6] RAPHIKA, P. M., ABDULLA, P., JASMINE, P. M. Planar elliptic function lowpass filter with sharp roll-off and wide stopband. *Microwave and Optical Technology Letters*, 2016, vol. 58, no. 1, p.133–136. DOI: 10.1002/mop.29520
- [7] REKHA, T. K., ABDULLA, P., RAPHIKA, P. M., et al. Compact microstrip lowpass filter with ultra-wide stopband using patch resonators and open stubs. *Progress In Electromagnetics Research C*, 2017, vol. 72, p. 15–28. DOI: 10.2528/PIERC16110202
- [8] BELBACHIR, A. K., BOUSSOUIS, M., TOUHAMI, N. A. High-performance LPF using coupled C-shape DGS and radial stub resonators for microwave mixer. *Progress In Electromagnetics Research Letters*, 2016, vol. 58, p. 97–103. DOI: 10.2528/PIERL15090105
- [9] HAYATI, M., EKHATERAEI, M., SHAMA, F. Compact lowpass filter with flat group delay using lattice-shaped resonator. *Electronics Letters*, 2017, vol. 53, no. 7, p. 475–476. DOI: 10.1049/el.2016.3431
- [10] KUMAR, L., PARIHAR, M. S. Compact hexagonal shape elliptical low pass filter with wide stop band. *IEEE Microwave Wireless Component Letters*, 2016, vol. 26, no. 12, p. 978–980. DOI: 10.1109/LMWC.2016.2623246
- [11] HOSEINABADI, A., TAVAKOLI, M. B., RASTEGAR FATEMI, M. J., et al. A new method for designing modified compact microstrip LPF with sharp roll-off and wide stopband. *Radioengineering*, 2021, vol. 30, no. 4, p. 662–669. DOI: 10.13164/re.2021.0662
- [12] MOLOUDIAN, G., BAHRAMI, S., HASHMI, R. M. A microstrip lowpass filter with wide tuning range and sharp roll-off response. *IEEE Transactions on Circuits and Systems II: Express Briefs*, 2020, vol. 67, no. 12, p. 2953–2957. DOI: 10.1109/TCSII.2020.2985206
- [13] TOMAR, P. S., PARIHAR, M. S. The design and investigation of the low-pass filter with high selectivity and ultra-wide stopband. *IETE Journal of Research*, 2023, p. 1–6. DOI: 10.1080/03772063.2023.2185303

## About the Authors ...

**Pankaj Singh TOMAR** received the B.E. degree in Electronics Engineering and M.Tech. degree in Microwave Engineering from RGPV, Bhopal, India. He is currently pursuing Ph.D. degree with the Department of Electronics and Communication Engineering, Indian Institute of Information Technology, Design and Manufacturing (IIITDM), Jabalpur, India. His current research interests include reconfigurable filters and antennas, microwave integrated circuits, and RF/microwave passive circuits and microwave and millimeter-wave device characterization.

**Manoj Singh PARIHAR** received the B.E. and M.Tech. degrees from RGPV, Bhopal, India, in 2001 and 2004, respectively, and the Ph.D. degree from IIT Delhi, New Delhi, India, in 2012. From 2010 to 2013, he was a Senior Project Scientist with the Center for Applied Research in Electronics (CARE), IIT Delhi. In 2007, he received an Institute of Electronics and Telecommunication Engineers (IETE) Research Fellowship for continuing his research work in reconfigurable antennas at IIT Delhi, and simultaneously, he was selected for the invitation program sponsored by the National Institute of International Education (NIIED) of the Ministry of Education and Human Resources of Republic of Korea to visit Korean universities and industries. He is currently an Assistant Professor with the Indian Institute of Information Technology, Design and Manufacturing (IIITDM), Jabalpur, India. His current research interests include reconfigurable antennas, microwave integrated circuits, microwave and millimeter-wave device characterization, and RF MEMS.

## Appendix A: Principle of Ground Slotting

The metallic patch of the circular slot in the ground plane acts as cylindrical cavity resonators and modeled as parallel stopband resonating circuit. The propagation along

normal direction is zero for cylindrical cavity resonator. As a result, the field components (E-electric field and H-magnetic field) inside the circular cavity are expressed by (A1)–(A4).

$$H_z = E_\theta = E_r = 0, \tag{A1}$$

$$E_z = k^2 J_n(kr) \cos(n\theta + \phi), \tag{A2}$$

$$H_r = \frac{j\omega\epsilon n}{r} J_n(kr) \sin(n\theta + \phi), \tag{A3}$$

$$H_\theta = j\omega\epsilon k J_n'(kr) \cos(n\theta + \phi) \tag{A4}$$

where  $J_n$  and  $k$  are the Bessel function of order  $n$  and cutoff wave number, respectively.

To find the condition of resonance and to calculate the resonance frequencies of expected modes, the expression of surface current ( $\mathbf{K}$ ) inside the slot on ground plane is determined as

$$\mathbf{K} = \mathbf{a}_N \times \mathbf{H}, \tag{A5}$$

$$\mathbf{K} = \mathbf{a}_z \times (H_r \mathbf{a}_r + H_\theta \mathbf{a}_\theta),$$

$$\mathbf{K} = (H_r \mathbf{a}_\theta - H_\theta \mathbf{a}_r). \tag{A6}$$

The radial component of the surface current  $K_r(r)$  at the edge of the plane inside the circular slot must vanish, therefore

$$H_\theta(r)|_{r=r_0} = 0 \text{ for all } \theta, \tag{A7}$$

$$J_n'(kr)|_{r=r_0} = 0 \tag{A8}$$

and using (A8) the radius of a particular (dominant) mode is defined as at resonance.

$$\text{For } n = 1, \quad kr_0 = 1.8411$$

$$r_0 = \frac{1.8411 f_r}{2\pi c \sqrt{\epsilon_r}}. \tag{A9}$$